

# NUMERICAL MODELING OF COASTAL DIKE OVERTOPPING USING SPH AND NON-HYDROSTATIC NLSW EQUATIONS

Philippe St-Germain<sup>1</sup>, Ioan Nistor<sup>2</sup>, John Readshaw<sup>3</sup> and Grant Lamont<sup>4</sup>

This paper evaluates the results of two fundamentally different numerical models: DualSPHysics and SWASH, which can be used to assess the ability of coastal defense structures to offset or mitigate the water overtopping and subsequent implications for expected future sea level rise. The models are open source implementations of the smoothed particle hydrodynamics (SPH) method and of a non-hydrostatic adaptation of the non-linear shallow water (NLSW) equations, respectively. The small-scale physical experiment of Stansby and Feng (2004) is used to validate and assess the performance of the two numerical models for the case of breaking monochromatic waves overtopping a coastal dike. Numerical and experimental time-histories of water surface elevation are quantitatively compared and numerical velocity fields during the processes of wave breaking and overtopping are analysed in detail. In addition, to further validate the DualSPHysics model, numerical experiments are performed considering the more realistic case of irregular waves using the SWASH model as benchmark. Overall, results provided by both numerical models are generally comparable, although some strengths and shortcomings of each are highlighted. These results can provide guidance in selecting the most appropriate model for a particular situation given specific accuracy requirements and availability of resources.

*Keywords: SPH method; non-linear shallow water equations; wave overtopping; coastal protection structure; sea level rise*

## INTRODUCTION

Climate change and the associated expected sea level rise will affect the performance of many existing coastal defence structures such as breakwaters, seawalls, and dikes, whose integrity under such changing conditions need to be reassessed. Reassessment will provide opportunities to consider alternatives that are “softer” in terms of armouring, and which can provide greater ecological services, with possible cost advantages (Lamont *et al.*, 2014). Soft alternatives generally include: beach nourishment, restoration or construction of dunes and wetlands; shore vegetation preservation or creation; and construction of (nearshore) reefs and berms as part of the shoreline system. Design guidance for soft alternatives is generally scarce, compared to more conventional structures, and numerical modeling appears to be a promising approach to overcome this gap. This paper evaluates and critically compares two fundamentally different numerical methods: the smoothed particle hydrodynamics (SPH) method and a non-hydrostatic adaptation of the non-linear shallow water (NLSW) equations with the goal of assessing their relative suitability for evaluating the implications of sea level rise and wave interaction with coastal structures.

The SPH method was first considered in 1994 to simulate general free-surface flows (Monaghan, 1994) by solving the full compressible Navier-Stokes equations. Shortly after, the method began to be applied to coastal flows (e.g., Monaghan and Kos, 1999). With the general exception of Didier and Neves (2009, 2010), the method has rarely been applied to wave-structure interaction scenarios in which a wide array of non-linear processes including wave propagation and transformation, breaking, run-up, and overtopping take place. Validation of the SPH method for practical purposes is still scarce, especially for the case of irregular waves.

On the other hand, the use of the NLSW equations for simulating coastal flows is not as new (e.g., Hibberd and Peregrine, 1979). The NLSW equations are derived from the incompressible Navier-Stokes equations assuming depth-averaged velocity and hydrostatic pressure. These equations are generally limited to deep and transitional water conditions as these assumptions do not hold during wave breaking. To overcome this limitation, numerous schemes accounting for non-hydrostatic pressure have been investigated (Casulli and Stelling, 1998; Stansby and Zhou, 1998) and one of them is considered in this paper.

In order to understand the capabilities and limitations of these two numerical methods for the case of breaking waves overtopping a coastal dike, 2D (vertical) numerical models are compared to

---

<sup>1</sup> Ports and Marine, SNC-Lavalin, 1800-1075 W. Georgia St., Vancouver, BC, V6E3C9, Canada, [philippe.st-germain@snclavalin.com](mailto:philippe.st-germain@snclavalin.com)

<sup>2</sup> Dpt. of Civil Eng., U. of Ottawa, 161 Louis-Pasteur, Ottawa, Ontario, K1N6N5, Canada, [inistor@uottawa.ca](mailto:inistor@uottawa.ca)

<sup>3</sup> Ports and Marine, SNC-Lavalin, 1800-1075 W. Georgia St., Vancouver, BC, V6E3C9, Canada, [john.readshaw@snclavalin.com](mailto:john.readshaw@snclavalin.com)

<sup>4</sup> Ports and Marine, SNC-Lavalin, 1800-1075 W. Georgia St., Vancouver, BC, V6E3C9, Canada, [grant.lamont@snclavalin.com](mailto:grant.lamont@snclavalin.com)

laboratory experiments and to one another. A brief summary of the small-scale physical experiment of Stansby and Feng (2004) is first provided as background to the assessment of the numerical models investigated in this paper. Next, the SPH and Non-hydrostatic NLSW equations methods are described. The results of each model, such as velocity fields during wave breaking and the resulting dike overtopping parameters are then compared, followed by a quantitative comparison with experimental results of time-history of the water surface elevation. Finally, additional numerical experiments performed considering the more realistic case of irregular waves are presented.

### EXPERIMENTAL SETUP

The physical experiment (Stansby and Feng, 2004) was performed in a 13m long, 0.3m wide, and 0.5m deep flume. Starting 1.9m from a piston-type wavemaker, a beach foreshore with a slope of 1V:20H ( $\tan \alpha = 0.05$ ) was installed and an impermeable trapezoidal dike (hereafter referred as “the structure”) was placed at its top (Fig. 1). The 0.1m high structure had a 0.2m wide horizontal crest and slopes of 1V:2H on both the seaward and landward sides. Monochromatic waves were generated by an almost sinusoidal wavemaker motion with a period  $T = 2.39$  sec in a water depth of  $d = 0.36$  m. Overtopping water was recirculated to the flume by means of pumping. Time-history of the water surface elevation was recorded using 12 wave gauges (denoted by “WG” in Fig. 1).

An overall description of the coastal flow emulated is as follows. Generated waves propagate onto the sloped beach, undergoing shoaling until they break and gradually develop into hydraulic bores. These bores subsequently impact and overtop the structure where partial wave reflection occurs. The reflected waves propagate back seaward, interacting with the incident waves.

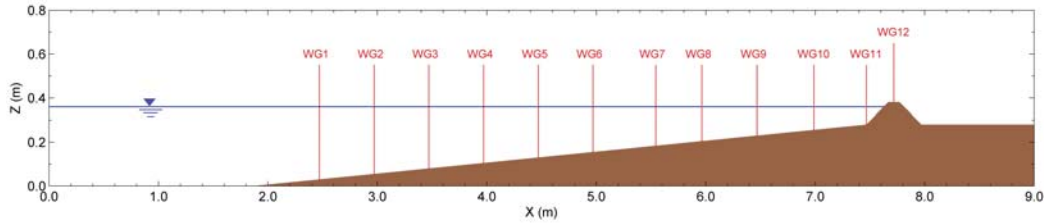


Figure 1. Side view of the experimental setup of Stansby and Feng (2004)

### NUMERICAL MODELS

The SPH and non-hydrostatic NLSW equations methods are described in the subsections below to highlight their differences. Provided also are details of their associated computational domains and parameters selected for the simulations performed. The later were based on a sensitivity analysis whose results are not included herein for sake of brevity. It should be noted that, from here onwards, the SPH and Non-hydrostatic NLSW equations methods will be referred to by the name of their respective computer codes which were used to perform the simulations.

#### DualSPHysics

Lagrangian SPH simulations were performed on the graphics processing unit (GPU) using the open source single-phase DualSPHysics implementation ([dual.sphysics.org](http://dual.sphysics.org)).

**Theoretical Background.** In the SPH method, the problem domain is discretized into a set of arbitrarily distributed points, or particles (Fig. 2, left), each of which has individual properties associated to them such as mass, density, velocity, pressure, etc., and which move according to prescribed governing equations. Since the formulation of the SPH method is not affected by the arbitrariness of the spatial distribution of the particles, the method can handle problems that include extremely large deformations without any special surface treatment. This is considered to be its most attractive feature. Numerical discretization involves approximating the values of functions at a certain particle using the information of the neighboring particles. Such approximation of a vector function  $\mathbf{f}$  at particle  $i$  is expressed in discrete form as:

$$\mathbf{f}(\mathbf{x}_i) = \sum_{j=1}^N \frac{m_j}{\rho_j} \mathbf{f}(\mathbf{x}_j) W(r_{ij}, h) \quad (1)$$

where  $\mathbf{x}_i$  is the position vector of particle  $i$  and  $\mathbf{x}_j$ ,  $m_j$ ,  $\rho_j$  are the position vector, mass, and density of a neighboring particle  $j$ , respectively;  $h$  is the smoothing length;  $r_{ij} = \|\mathbf{x}_i - \mathbf{x}_j\|$  is the distance separating particle  $j$  from particle  $i$ ;  $W$  is a weighting function or the so-called “smoothing kernel”. As shown in Fig. 2 (right), the smoothing length controls the size of the influence domain  $\Omega$  of particle  $i$ , the region

containing the  $N$  neighboring particles that contributes to the approximation. Applying the approximation to discretize the compressible Navier-Stokes equations of continuity and momentum, the following governing equations are obtained, respectively:

$$\frac{D\rho_i}{Dt} = \rho_i \sum_{j=1}^N \frac{m_j}{\rho_j} (\mathbf{u}_i - \mathbf{u}_j) \cdot \nabla_i W(r_{ij}, h) \quad (2)$$

$$\frac{D\mathbf{u}_i}{Dt} = - \sum_{j=1}^N m_j \left( \frac{P_i + P_j}{\rho_i \rho_j} \right) \nabla_i W(r_{ij}, h) + \mathbf{g} + \boldsymbol{\theta} \quad (3)$$

where  $\mathbf{u}_i$ ,  $\mathbf{u}_j$ ,  $P_i$ , and  $P_j$  are the velocity vectors and pressures of particles  $i$  and  $j$ , respectively, and  $\mathbf{g}$  is the gravitational acceleration vector. The diffusion terms  $\boldsymbol{\theta}$  of the momentum equation are modeled according to the laminar viscosity with the Sub-Particle Scale (SPS) turbulence formulation proposed by Dalrymple and Rogers (2006). In order to calculate the pressure terms of the momentum equation, the fluid is treated as weakly compressible and the equation of state proposed by Monaghan (1994) is used:

$$P_i = \frac{c_0^2 \rho_0}{\gamma} \left[ \left( \frac{\rho_i}{\rho_0} \right)^\gamma - 1 \right] \quad (4)$$

where  $\gamma = 7$  is a constant,  $\rho_0 = 1000 \text{ kg/m}^3$  is the reference water density, and  $c_0$  is the speed of sound in water at the reference density. For further details on the SPH method and its implementation in DualSPHysics, the reader is referred to Crespo *et al.* (2013).

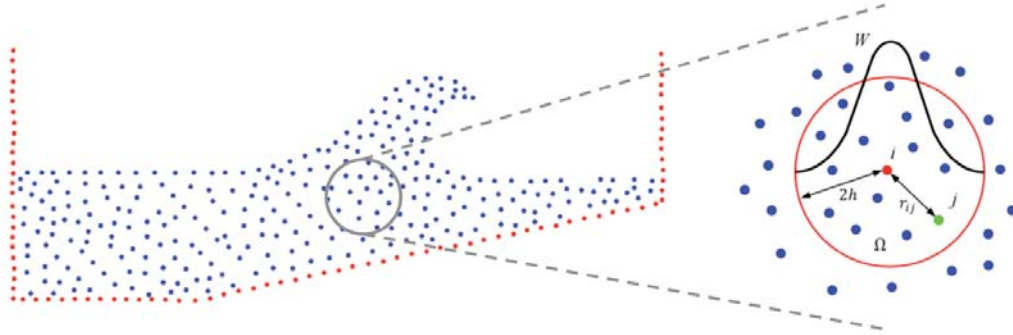


Figure 2. Schematics of SPH grid-free domain discretization (left) and influence domain of function approximation at particle  $i$  (right)

**Computational Domain and Simulation Parameters.** An inter-particle spacing of 0.005 m was used and the total number of particles was  $\sim 150,000$ . The flume boundaries, beach, wavemaker, and structure were modeled by perfectly fixed dynamic boundary particles (Dalrymple and Knio, 2001). The Wendland (1995) smoothing kernel formulation was considered along with  $h = 0.006$  m. For advancing the simulation, the Verlet (1967) time integration algorithm was considered and a Shepard density filter was applied every 25 time steps to prevent fluctuations in the pressure field. No XSPH correction (Monaghan, 1994) was applied as it was observed to cause unrealistic cross-shore currents after longer simulation times. The simulation was performed on a Nvidia Tesla C2050 GPU with 448 cores and  $\sim 4$  hours of computational time was required to simulate 60 sec of the physical experiment.

The configuration of the DualSPHysics computational domain is shown in Fig. 3. To generate the same waves as the ones in the physical experiment, a numerical piston-type wavemaker was located just seaward of WG1 (see Fig. 1) and the Fourier transform-based procedure of Carvalho (1989) was used to pre-derive a ramped wavemaker motion from the experimental wave signal. To allow water recirculation, as in the physical experiment, a 0.05 m diameter conduit was modeled connecting the back area of the structure to the flume.

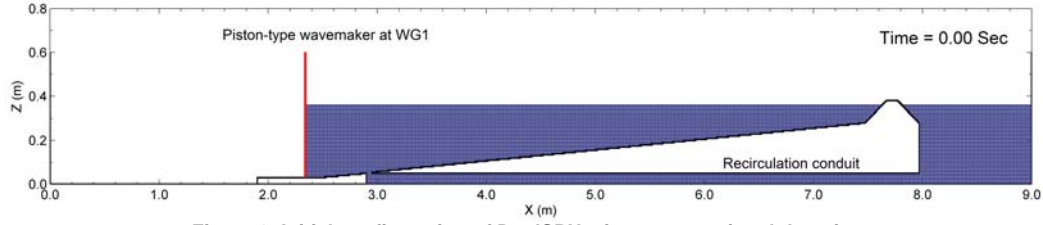


Figure 3. Initial configuration of DualSPHysics computational domain

### SWASH

For the non-hydrostatic NLSW equations method, the open source single-phase SWASH implementation ([swash.sourceforge.net](http://swash.sourceforge.net)) was utilized.

**Theoretical Background.** Derived from the incompressible Navier-Stokes equations, the governing equations considered in this study are the NLSW equations of continuity and momentum including non-hydrostatic pressure terms, in both horizontal and vertical directions:

$$\frac{\partial u}{\partial x} + \frac{\partial w}{\partial z} = 0 \quad (5)$$

$$\frac{\partial u}{\partial t} + \frac{\partial u^2}{\partial x} + \frac{\partial wu}{\partial z} + \frac{1}{\rho} \frac{\partial (P_h + P_{nh})}{\partial x} + c_f \frac{u|u|}{h} = \frac{\partial \tau_{xx}}{\partial x} + \frac{\partial \tau_{xz}}{\partial z} \quad (6)$$

$$\frac{\partial w}{\partial t} + \frac{\partial uw}{\partial x} + \frac{\partial w^2}{\partial z} + \frac{1}{\rho} \frac{\partial P_{nh}}{\partial z} = \frac{\partial \tau_{zx}}{\partial x} + \frac{\partial \tau_{zz}}{\partial z} \quad (7)$$

where  $u$  and  $w$  are the horizontal and vertical flow velocities, respectively;  $P_h$  and  $P_{nh}$  are the hydrostatic and non-hydrostatic pressure components, respectively;  $\tau_{xx}$ ,  $\tau_{xz}$ ,  $\tau_{zx}$ , and  $\tau_{zz}$  are the turbulent stresses;  $c_f = n^2 g / \sqrt[3]{h}$  is a bottom friction coefficient based on Manning's  $n = 0.002$ ; and  $\rho = 1000 \text{ kg/m}^3$  is the density of water. As depicted in Fig. 4 (left)  $h = \eta + d$  is the total water depth with  $\eta$  and  $d$  being the water surface and bottom depth above and below still water level (SWL), respectively. By considering the mass balance through the water column, the water surface can be obtained by:

$$\frac{\partial \eta}{\partial t} + \frac{\partial}{\partial x} \int_{-d}^{\eta} u dz = 0 \quad (8)$$

To solve the above set of governing equations, the problem domain is discretized into a grid of constant horizontal spacing  $\Delta x$  with equally-distributed boundary-fitted vertical layers as shown in Fig. 4 (right). This vertical discretization, for which flow properties are averaged over the variable height of each layer, enables the computation of vertical accelerations and vertical pressure gradients resulting in accurate frequency dispersion (Zijlema and Stelling, 2008). Using a sufficient number  $K$  of vertical layers, this scheme is able to reproduce the entire wave breaking process and the associated energy dissipation without any additional breaking formulation. The reader is referred to Zijlema *et al.* (2011) for additional theoretical details of SWASH.

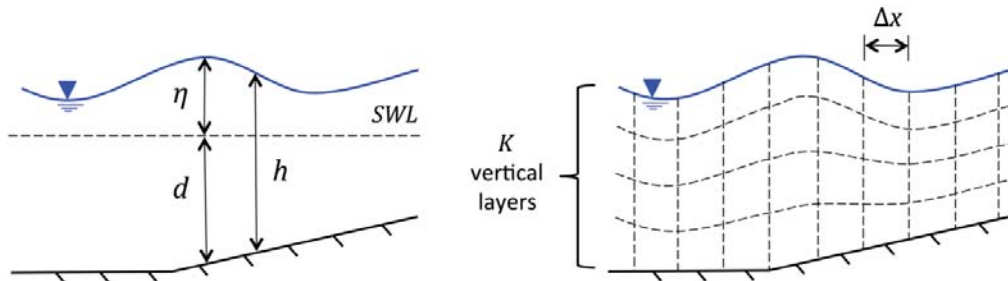


Figure 4. Schematics of SWASH definition of free surface (left) and grid domain discretization (right)

**Computational Domain and Simulation Parameters.** The configuration of the SWASH computational domain is shown in Fig. 5. The SWASH computational domain started seaward at WG1 (see Fig. 1), where the ramped experimental wave signal was imposed through a weakly reflective boundary condition allowing outgoing reflected waves. A simple radiation boundary condition was used for the landward side of the computational domain. Such open side boundaries eliminated the need for overtopping water recirculation by keeping the seaward water level constant.

The computational grid had spacing of  $\Delta x = 0.02\text{m}$  and  $K = 15$ . A momentum-conservative backward difference (BDF) numerical discretization scheme was used to solve the governing equations across the computational grid and the non-hydrostatic pressure terms were calculated via a Poisson equation solved using a BiCGSTAB solver pre-conditioned with incomplete LU factorization. Lastly, the simulation was advanced in time according to a 2<sup>nd</sup> order leapfrog scheme and the turbulent stresses terms of the momentum equations were described using a  $k\text{-}\epsilon$  turbulence model.

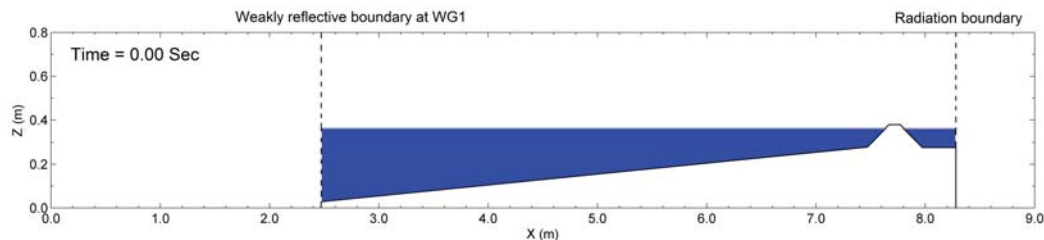


Figure 5. Initial configuration of SWASH computational domain

## RESULTS

In the following three (3) subsections, numerical velocity fields from both models are compared, providing a visual description of the simulations; numerical predictions of water surface elevation are compared quantitatively to experimental measurements, validating the numerical results; and numerical experiments performed considering the more realistic case of irregular waves are presented.

### Numerical Velocity Fields

**Wave breaking.** The numerical surf similarity parameter was estimated to  $\xi_b = \tan \alpha / \sqrt{H_b/L_0} \approx 0.3$ . This value is close to the limit of 0.4 between spilling and plunging breakers (Battjes, 1974). The breaking wave height  $H_b \approx 0.2$  m was obtained from DualSPHysics water surface predictions while the deep water wave length  $L_0 = gT^2/2\pi = 9.0$  m was taken as the wave length seaward of the beach according to linear wave theory with  $T = 2.39$  sec. Comparable  $\xi_b$  were computed based on experimental water surface measurements and SWASH predictions.

Through the wave breaking process, from incipient breaking to hydraulic bore formation, Fig. 6 shows a time sequence of side-by-side numerical velocity fields predicted by the two numerical models. In this figure and the subsequent ones, the color scale indicates the magnitude of the flow velocity while the arrow vectors indicate flow direction. It should be noted that, due to a small  $\sim 0.15$  sec time lag generally observed between the DualSPHysics and SWASH results, the times of the velocity fields were selected such that latter were corresponding from a wave progression standpoint. Such time lag will be further discussed in the following subsection in which numerical results of water surface are compared to experimental ones.

It is clear that DualSPHysics provides a better representation of the energetic wave breaking process by capturing the formation of a weak plunging jet, spilling, and splash-up followed by strong turbulent mixing. This mixing is characterized by the formation coherent vortices occurring in pairs and rotating in opposite directions near the bottom (Fig. 6g). Although dissipated by viscosity, these vortices remain until the arrival of a subsequent wave (Fig. 6a) before being broken down by the seaward current at the wave front (e.g., Fig. 6c). Although the breaker in Fig. 6 appears visually to be weakly plunging, it was noticed through video analysis of the DualSPHysics velocity fields that the breaking type varied from spilling to plunging and that the breaking location slightly varied ( $X = 4.85 \pm 0.15$  m) also from one wave to another. The breaking location is defined herein as the location where the shoaling ceases and the wave height begins reducing (i.e., maximum wave height). Also, vortices were observed to become more extensive as waves become more plunging.

In the case of SWASH, the breaking process is simulated quite differently. The wave is observed to shoal with its front steepening until it becomes too steep, after which its height reduces gradually and its form changes into the one of a steady bore accordingly. More specifically, the observed

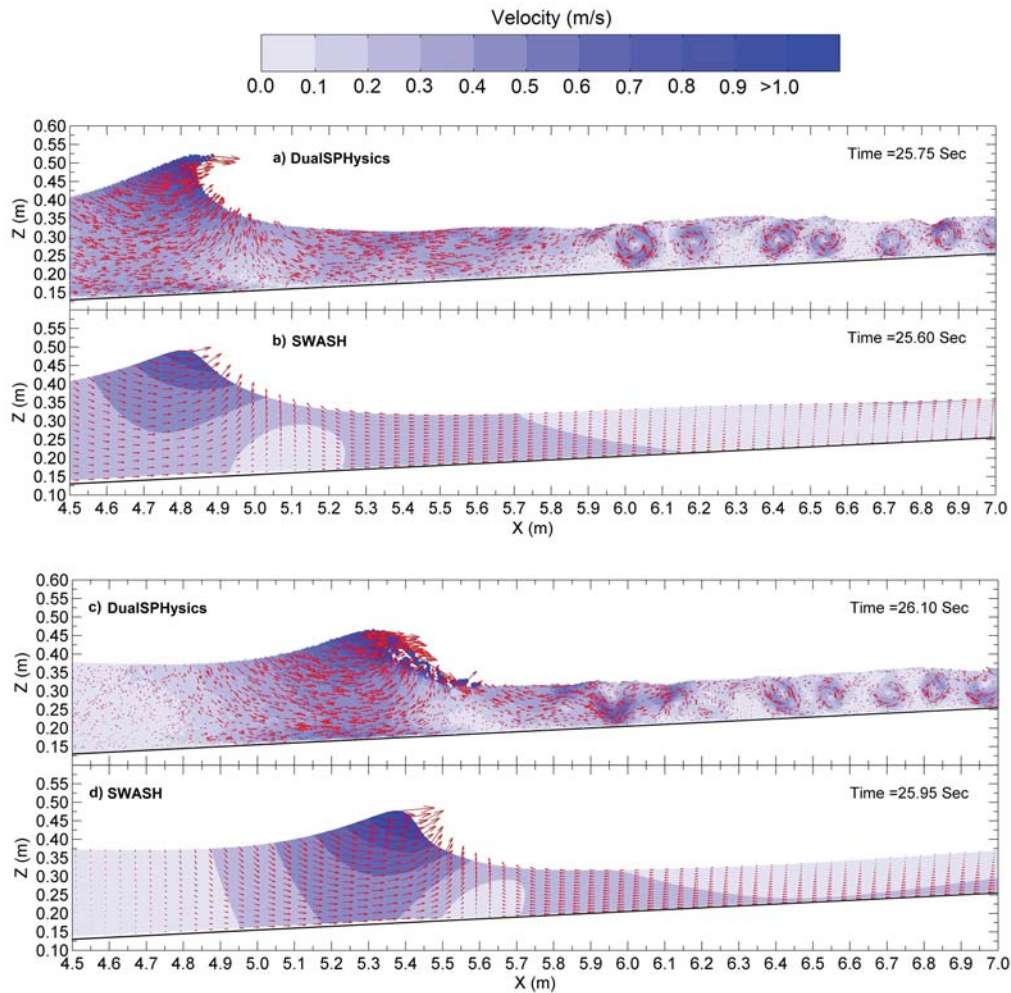


Figure 6. See next page for caption

steepening of the wave front is balanced by the deviation from hydrostatic pressure, stabilizing the surface profile preventing it to become vertical (Stelling and Zijlema, 2010). Based on the analogy with hydraulic jumps and by ensuring conservation of momentum, energy dissipation of the wavebreaker-generated turbulence on the front face of the wave is inherently accounted for (e.g., Zijlema *et al.*, 2011), resulting in this gradual reduction in wave height. Also, the location of incipient breaking ( $X = 4.85$  m) and the overall breaking process are much more constant from one wave to another compared to DualSPHysics.

Although visual comparison of the numerical velocity fields shown in Fig. 6 shows striking differences, similarities can also be observed. Apart from water surface deformation and turbulent vortices, the regions of high and low velocities predicted by the numerical models are in reasonably good agreement. Considering Fig. 6a and Fig. 6b for instance, a near-bed stagnation point just landward of the wave crest is clearly visible for both numerical models, where landward and seaward flows converge and are reoriented upwards. Agreement is also observed in the forward velocity at the wave crest and its gradual decrease with increasing depth, as well as in the region of low velocity at the landward edge of the velocity field frame, with the exception of the vortices structures predicted by DualSPHysics.

Looking more closely at the flow velocity predicted by the numerical models, Fig. 7 provides the time-history of the near-bed flow velocity at the location of WG6 and WG8. Respectively, these correspond to the approximate location of incipient breaking and a location further seaward where breaking induces important mixing. For DualSPHysics, the flow velocity at the location of interest is calculated from the velocity of close-by particles by applying the approximation described by Eq. 1, while in the case of SWASH, it is determined by linear interpolation of the velocity at nearby grid

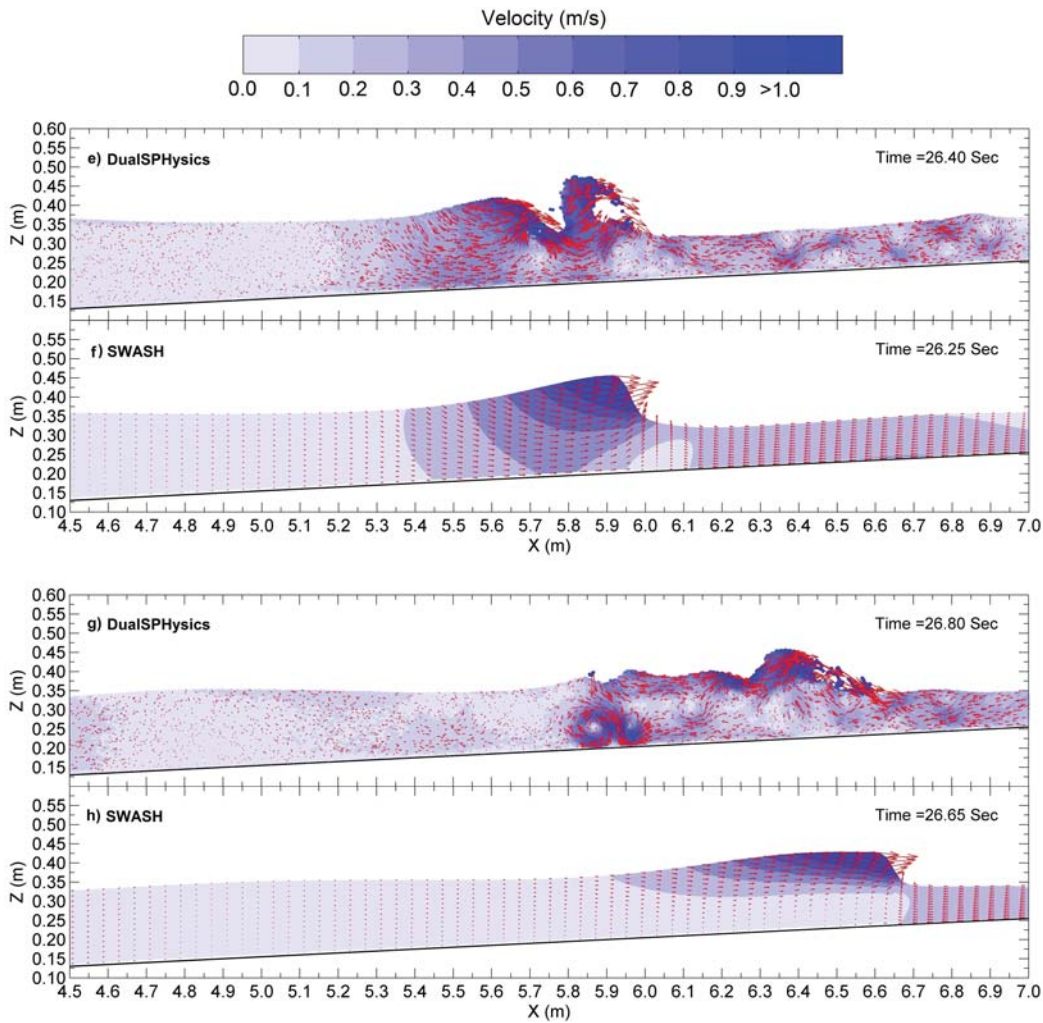


Figure 6. Comparison of DualSPHysics and SWASH numerical velocity field during wave breaking

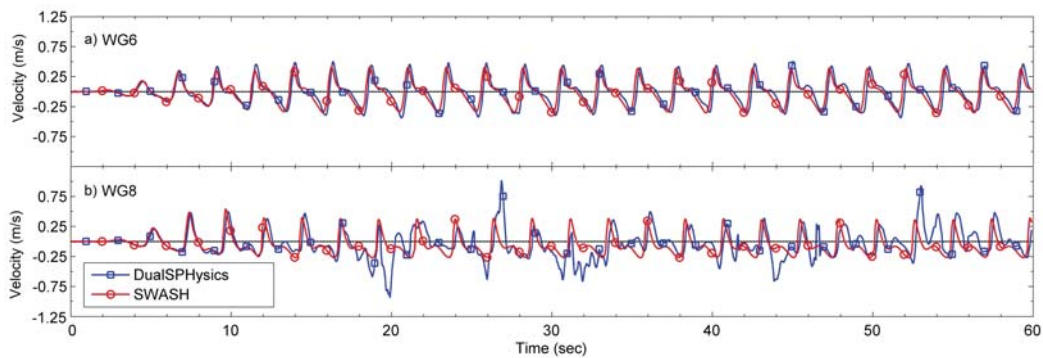


Figure 7. Comparison of DualSPHysics and SWASH numerical near-bed velocity time-history at wave gauges WG6 and WG8

nodes. Before and up to incipient breaking (Fig. 7a and Fig. 7b), there is very good agreement between the numerical models and some symmetry between landward- and seaward-directed velocities is observed, indicating little onshore mass drift. On the other hand, beyond breaking, some differences arise in the predictions by the numerical models. The velocity spikes in the DualSPHysics results are explained by the turbulent vortices the model reproduces (e.g., Fig. 6g), with the positive (i.e., landward) and negative (i.e., seaward) velocities associated to counter-clockwise and clockwise

vortices respectively. As the breaking location varied slightly in the DualSPHysics simulation, the vortices' location varied accordingly, explaining the intermittent spikes observed in Fig. 7b.

**Wave overtopping.** Following breaking, waves transform into hydraulic bores that subsequently impact and overtop the dike structure. Such bore-structure interaction is depicted in Fig. 8, which shows a time sequence of side-by-side numerical velocity fields predicted by the numerical models. Prior to impact (Fig. 8a and Fig. 8b), differences in the water surface profile of the incident hydraulic bores are observed: the DualSPHysics profile is undulated and the bore front is plunging forward. Shortly after impact (Fig. 8c and Fig. 8d), as water overtops the structure, the agreement in the numerical water surface profiles improves, although some flow separation from the structure's crest is observed for DualSPHysics. This can be explained by the fact that, due to the formulation of the SWASH model and the shallow water equations in general, the water medium cannot separate from the solid bottom boundary. Throughout the remainder of the bore-structure interaction (Fig. 8e to Fig. 8j), the water surface profiles predicted by the numerical models are quite similar.

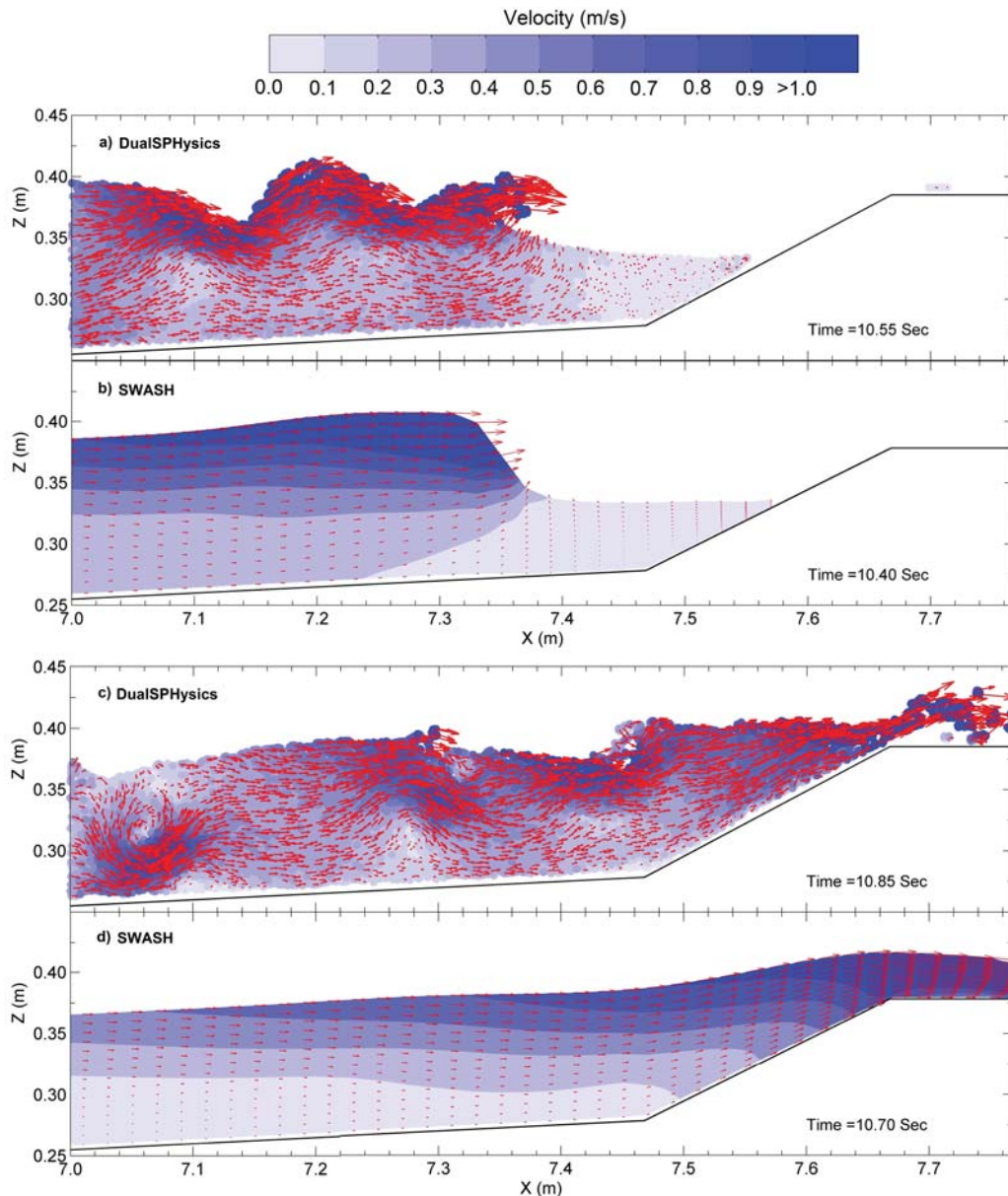


Figure 8. See page 10 for caption

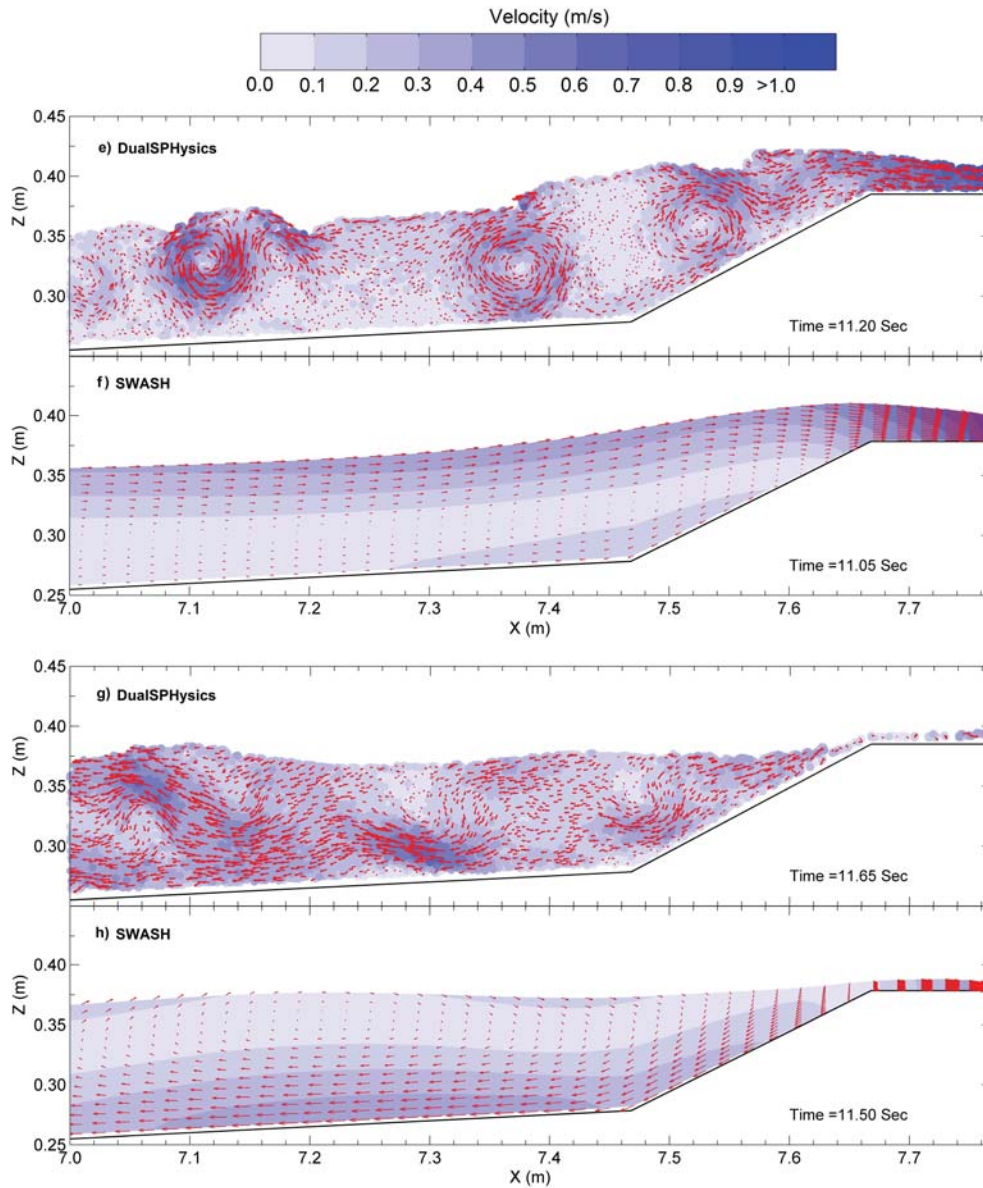


Figure 8. See page 10 for caption

During runoff, the SWASH velocity field (Fig. 8d) is generally horizontal, with lower near-bed velocities seaward of the structure's toe gradually increasing towards the surface and the leading edge of the flow over the structure. On the other hand, seaward of the structure, the DualSPHysics velocity field (Fig. 8c) displays less defined velocity gradients and distinct regions of higher velocities. At the beginning of rundown, these regions of higher velocities evolved into well-defined vortices (Fig. 8e). At that time also, the landward velocity of the leading edge of the flow over the structure decreases and seaward bottom velocities at the toe of the structure begin to develop. The latter is better noticeable in the case of SWASH (Fig. 8f), as landward surface velocities and seaward bottom velocities are clearly separated by a shear layer of low velocity. For both numerical models and further during rundown (Fig. 8g and Fig. 8h), the entire flow reverses to the seaward direction with stronger velocities towards the bottom. Once again, the DualSPHysics velocity field appears to be more irregular with undulations in the streamlines. In addition, a reflected wave near the seaward edge of the velocity field frame is seen. Lastly, towards the end of rundown, it can be noticed that, in the case of DualSPHysics (Fig. 8i), some particles remain essentially immobile on the crest of the dike resulting from the separation of landward overtopping and seaward rundown flows.

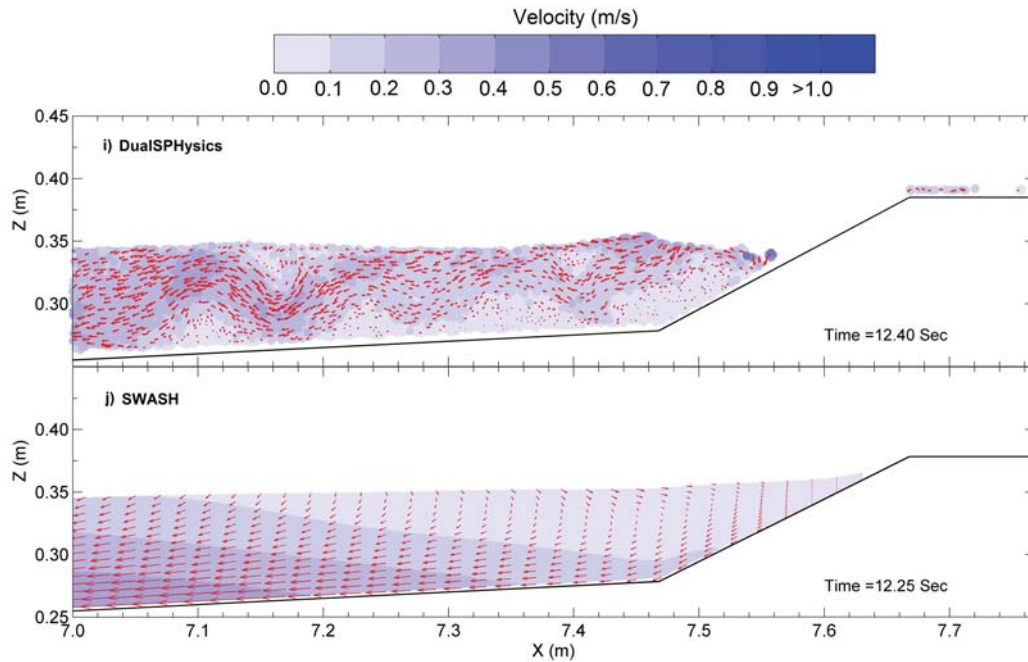


Figure 8. Comparison of DualSPHysics and SWASH numerical velocity field during dike overtopping

Fig. 9 provides the time-history of the near-bed flow velocity at the toe, mid-slope, and top (i.e., crest) of the dike structure computed by the numerical models. At the toe of the structure (Fig. 9a), the agreement between the models is marginal, with a clear tendency for SWASH to predict high upslope velocities (i.e., positive) compared to lower downslope velocities (i.e., negative). In the case of DualSPHysics, at simulation times beyond the ones shown in Fig. 8 (i.e., beyond ~20 sec), the velocities do not generally appear to follow a specific trend although they are more symmetrical with respect to upslope and downslope directions. This can be attributed to the turbulent vortices that are reproduced by the model, and similar to the wave breaking process, the location of these vortices varied from wave to wave. Midway along the seaward slope (Fig. 9b) and over the crest (Fig. 9c) of the structure, better agreement is observed between the numerical models.

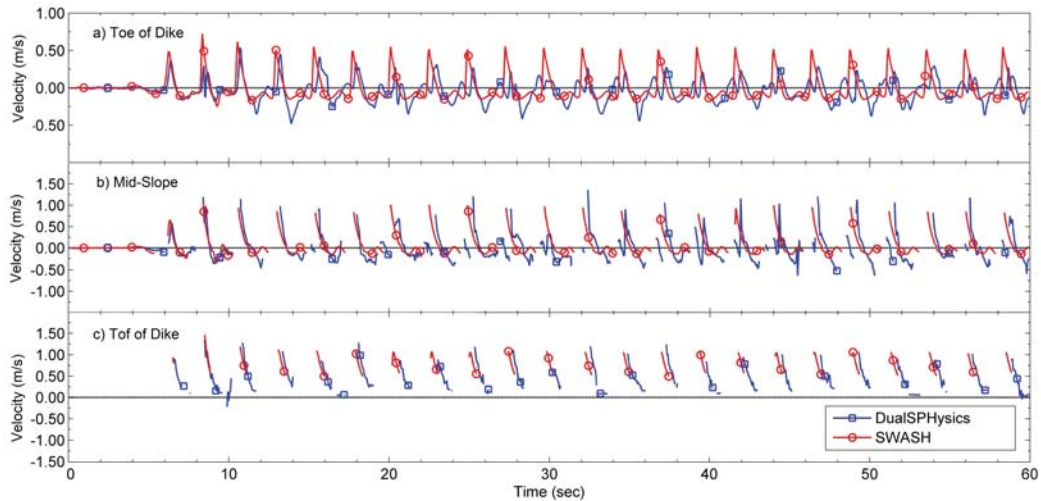


Figure 9. Comparison of DualSPHysics and SWASH numerical near-bed velocity time-history at the toe, mid seaward slope, and top of the dike

### Comparison with Physical Experiment

**Water surface elevation.** Fig. 10 shows a comparison of numerical and experimental time-history of the water surface elevation at various wave gauges, in which the vertical datum corresponds to the flat bottom of the experimental flume. Near the toe of the sloped beach foreshore (WG1), where the computational domains begin, the wave signal is to some extent sinusoidal with the exception of the double-peaked wave crest (Fig. 10a). While the comparison between SWASH and experimental results is quite good, some discrepancy is observed in the wave trough of the DualSPHysics time-history prediction. This is likely associated to the fact that, in the DualSPHysics model, waves are generated by the motion of a wavemaker located essentially just seaward of WG1, suggesting that wave form has not yet fully developed before reaching the wave gauge. On the other hand, in the case of SWASH, the experimental water surface elevation signal is imposed at the model's open boundary and the model computes associated boundary input flow velocities. This results in a more developed wave form starting right from the computational domain's offshore boundary, explaining thus why it compares better with the physical results at this location. Nevertheless, further landwards at WG4 (Fig. 10b), seaward of the breaking zone and where non-linear shallow water effects have altered the sinusoidal-like wave form, both numerical models results are in quite good agreement with the physical experiment ones, although it can be noticed that SWASH exhibits a small time lag of  $\sim 0.15$  sec. This time lag is generally sustained during the remainder of the wave propagation and suggests the prediction of a slower wave speed.

By analysis of the water surface elevation time-history at WG4 to WG8, which span the breaking zone, several observations are made. First, based on the good agreement of the numerical models' results with the physical experiment ones at locations before (WG4, Fig. 10b) and beyond breaking (WG8, Fig. 10f), it can be concluded that both numerical models simulate well the overall breaking process in terms of reduction in wave height and energy dissipation.

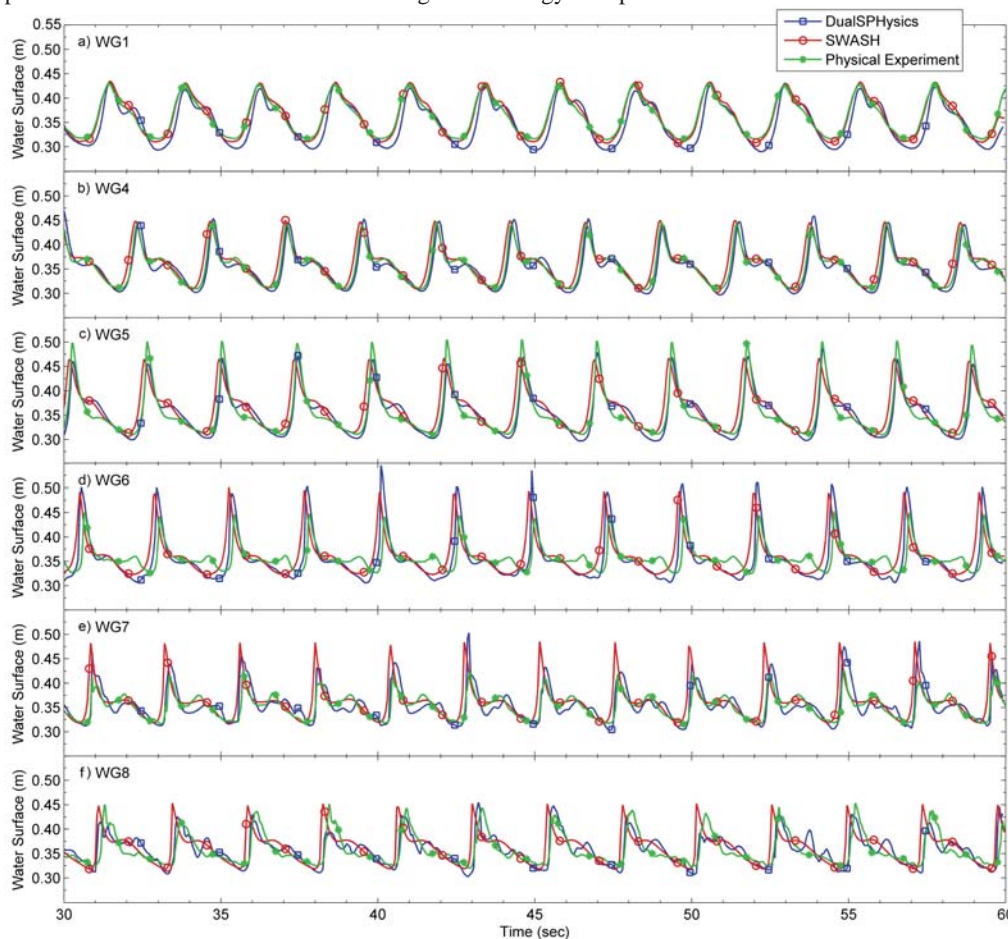
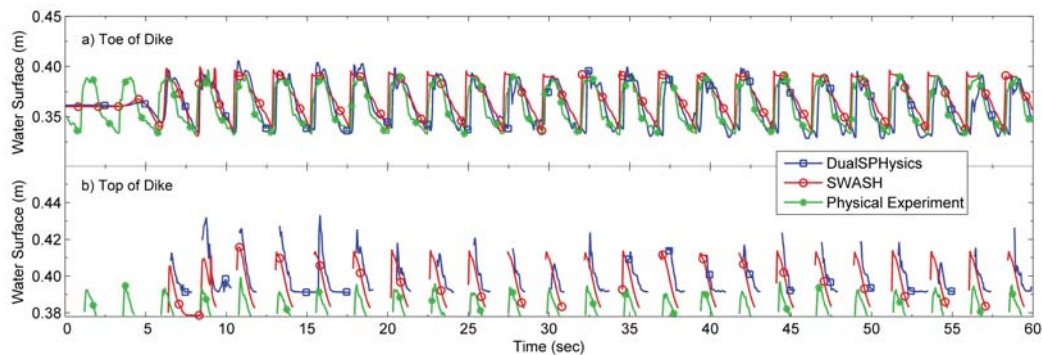


Figure 10. Comparison of numerical and experimental time-history of the water surface elevation at wave gauges WG1, WG4, WG5, WG6, WG7, and WG8

Looking at WG5 (Fig. 10c) and WG6 (Fig. 10d) results in more detail, based on the sudden reduction in the experimental wave height, wave breaking in the physical experiment is observed to occur more seaward compared to both numerical simulations. In the former, breaking initiated at WG5 ( $X = 4.47$  m), corresponding to the location where maximum wave height was physically observed (Stansby and Feng, 2004). On the other hand, as discussed previously, maximum wave height occurs further landward ( $X = 4.85$  m) in both numerical simulations, as determined by video analysis, and wave reduction can only be observed starting from WG6 ( $X = 4.97$  m) in the numerical time-histories of the water surface elevation shown in Fig. 10. Comparison of the numerical wave heights at WG6 and WG7 shows that the reduction in the wave height due to breaking is, as in the physical experiment, rather sudden for DualSPHysics, but more gradual in the case of SWASH.

A secondary peak at WG7 (Fig. 10e) occurs in both numerical models as well as in the physical experiment and can be associated with the waves reflected from the dike structure. At WG5 (Fig. 10c) and WG6 (Fig. 10d), although there is good agreement between the numerical models, there is some discrepancy with the physical measurements with respect to the wave trough. This may suggest that the numerical models reproduce differently the propagation of the reflected waves and consequently their interaction with the incident waves also. This could also explain the disagreement in the breaking location mentioned above, as the inception of wave breaking can be influenced by the superimposition of the incident waves with reflected waves.

Fig. 11 shows a comparison of numerical and experimental time-history of the water surface elevation at the toe (Fig. 11a) and on the top (i.e., crest) of the structure (Fig. 11b) where the interaction of the incident bores with the dike structure occurs. At the toe, there is good agreement between the physical measurements and the numerical predictions of both models, further supporting the fact that these reproduce properly the wave propagation and transformation occurring on the foreshore. Considering the water surface elevation, or overtopping flow depth, over the crest of the structure, the predictions of the numerical models are in reasonably good agreement. It can be noticed however that the water surface elevation predicted by DualSPHysics tends to slightly surpass the one from SWASH. This is attributed to the fact that, because of the incident bore's momentum as it runs up the seaward slope of the structure, the overtopping flow initially separates from the crest's surface in the case of DualSPHysics and reaches higher elevations over the dike's crest. Nevertheless, the numerical results differ significantly from the experimental ones. Interestingly, the same discrepancy was also noticed by Stansby and Feng (2004) and Oliveira *et al.* (2012), who applied a 1D depth-averaged, semi-implicit, finite-volume, shallow-water Boussinesq model (Stansby, 2003), and a 2D (vertical) Particle Finite Element Method (PFEM) model, respectively, to simulate the same physical experiment. The exact explanation for this discrepancy remains unknown at this stage and further investigation considering results from additional physical experiments will be undertaken to thoroughly validate the numerical models with respect to the overtopping process.



**Figure 11. Comparison of numerical and experimental time-history of the water surface elevation at the toe (WG11) and on the top of the dike (WG12)**

It can be noticed in Fig. 11b that, in the beginning of the DualSPHysics simulation (before ~20 sec), the overtopping flow depth over the dike crest is the largest of the two models. Video analysis of the DualSPHysics velocity fields showed that a few waves were required to build-up the turbulence in the foreshore region landward of the breaking location (e.g., Fig. 6a). Already present vortices in this region were noticed to further increase the turbulence of the hydraulic bores resulting from the breaking of subsequent waves, further dissipating the energy available to overtop the structure. The

latter also explains the previously discussed generally more random velocity pattern in Fig. 9a beyond ~20 sec.

**Overtopping volume.** By integrating the time-history of the product of the water depth and the depth-averaged flow velocity over the structure, the overtopping volume per meter width of structure was estimated. Fig. 12 shows that both numerical models show good agreement in the prediction of the overtopping volume over the entire duration of the simulations. However, the rate at which the overtopping volume increases appears more uniform in the case SWASH comparing to that of DualSPHysics. This is associated with the wave breaking and bore propagation that were observed to be more regular in the SWASH simulation compared to DualSPHysics. In the case of the latter, the time-history of the overtopping volume is characterized by more rapid initial increase rate followed by a slower one beyond ~20 sec. This suggests that had the simulation time been longer, SWASH would have predicted greater overtopping volume (and hence a greater mean overtopping discharge) than DualSPHysics. Since the overtopping flow velocities and depths compared relatively well between the two numerical models (Fig. 9c and Fig. 11b, respectively), more analysis is required to explain this difference, especially in addressing the way the overtopping volume is post-processed given the flow separation from the dike crest's in the case of DualSPHysics. (e.g., Fig. 8c).

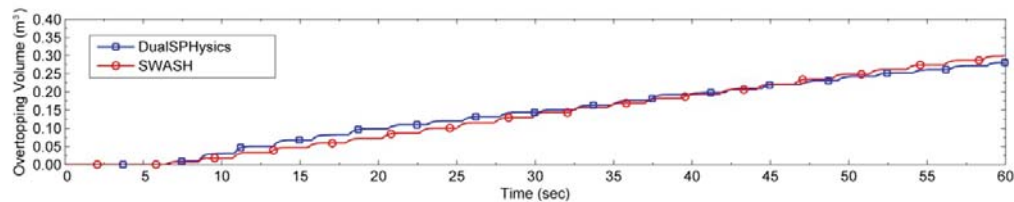


Figure 12. . Comparison of DualSPHysics and SWASH numerical time-history of the overtopping volume per meter width of dike structure

#### Numerical Modeling with Irregular Waves

To investigate the ability of DualSPHysics to simulate irregular waves in the surf zone, results from SWASH, which has already been validated against experimental data (Zijlema and Stelling, 2008), are used as reference. SWASH was used to generate a wave signal with  $H_s = 0.08$  m and  $T_p = 2.5$  sec according to a Jonswap spectrum with a  $\gamma = 3.3$  peak enhancement factor. A simulation time of 300 seconds was considered for the duration of this numerical experiment in order to generate a sufficient number of waves from a statistical viewpoint. The SWASH wave signal was converted into wavemaker motion as input into the DualSPHysics model by means of the Fourier transform-based approach of Carvalho (1989).

Fig. 13 shows that DualSPHysics compares well with results computed by SWASH at several wave gauges along the surf zone. Seaward of the location where breaking begins (Fig. 13a), there is a larger distribution of the wave height, but further landward, the wave height is clearly depth-limited (Fig. 13c). The gradual reduction in wave energy due to wave breaking can be observed in Fig. 14, which shows energy density spectra at the location of the wave gauges considered in Fig 13. Generally, DualSPHysics reproduces well the wave spectra of SWASH. Two peaks at  $f = 0.38$  Hz and  $f = 0.85$  Hz are visible. The low frequency peak is associated to the incoming waves from the seaward domain boundary as it corresponds to the peak period that was specified as input. The higher frequency peak is believed to be associated with the partial wave reflection that occurs within the numerical flume.

#### CONCLUSIONS

As part of this comprehensive research work to identify appropriate numerical tools for the performance assessment of coastal defence structures, DualSPHysics and SWASH, open source implementations of the SPH method and of the non-hydrostatic NLSW equations, respectively, were employed to simulate a coastal dike overtopping scenario that involved wave propagation, transformation, breaking, and reflection. Although the numerical models considered are fundamentally different in terms of spatial and numerical discretization, the results they provided are generally comparable.

For the case of monochromatic waves, quantitative comparison of the numerical results with physical measurements of water surface elevation along the foreshore indicates that both models simulate correctly the magnitude and rate of reduction in wave height and energy dissipation associated with the wave breaking process. This infers that both models can be confidently applied to estimate

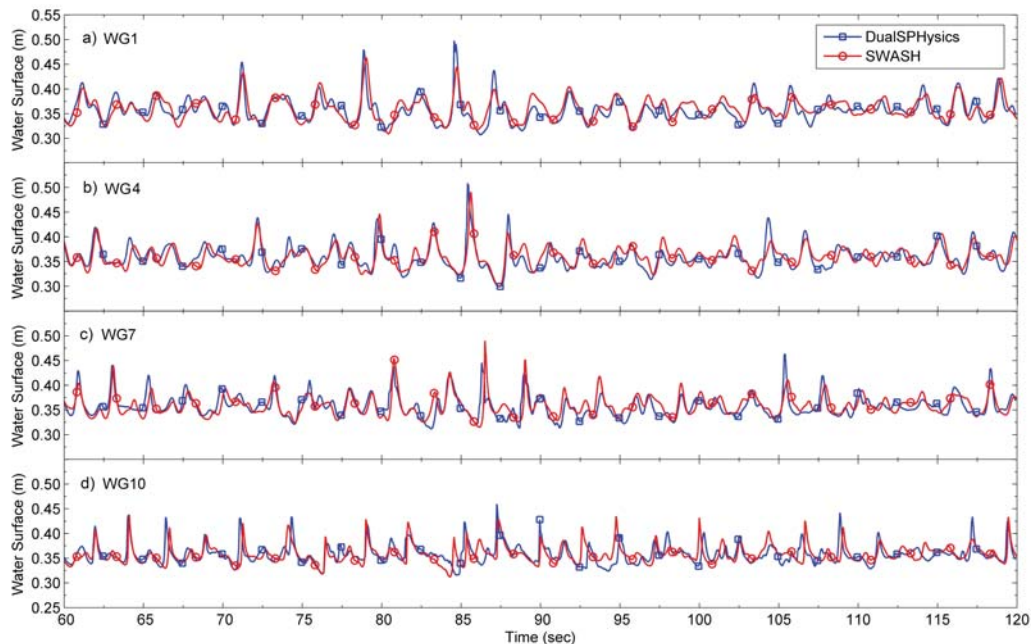


Figure 13. Comparison of DualSPHysics and SWASH numerical time-history of the water surface elevation at wave gauges WG3, WG9, WG10, and WG11 for the case of irregular waves

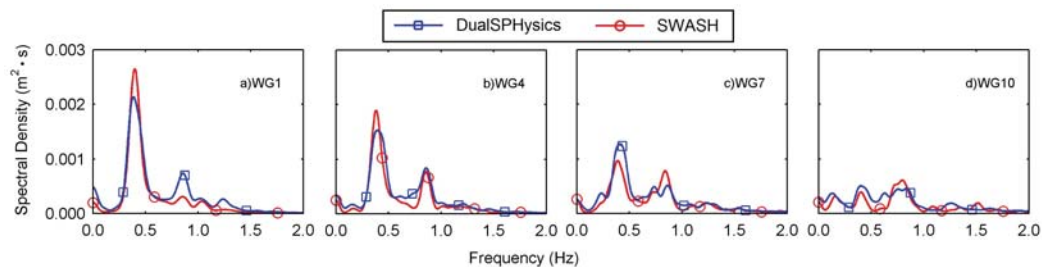


Figure 14. Comparison of DualSPHysics and SWASH irregular wave spectra at wave gauges WG1, WG4, WG7, and WG10.

incident wave heights for design purposes. Also, numerical experiments using SWASH as reference demonstrated that DualSPHysics is also capable of handling irregular waves and their transformation in the surfzone. Nevertheless, analysis of numerical velocity fields showed that the way the breaking process is actually modeled differs significantly between the two models. More specifically, DualSPHysics provided a more realistic representation of the energetic wave breaking process by reproducing wave plunging, spilling, and splash-up followed by strong turbulent mixing indicated by the formation of coherent vortices. This suggests that if a problem of interest occurs within the breaking zone – from incipient breaking to the hydraulic bore formation – SWASH may provide less accurate results compared to DualSPHysics. For instance, if dealing with scour protection within the breaking zone, it would be important to take into account the higher flow velocities associated to the turbulent vortices captured by DualSPHysics but not by SWASH.

An impermeable trapezoidal coastal dike structure was used to assess the overtopping predictions by both numerical models. The numerical results of the overtopping flow velocity and depth over the crest of the structure were in reasonable agreement. Although this needs to be verified, it is hypothesized that, for the estimation of overtopping, SWASH may be less applicable as the spray component of the overtopping flow becomes more important. This is because the nature of SWASH and of the shallow water equations in general does not permit flow separation from the bottom solid boundary.

From a usability point of view, SWASH was generally easier to setup in terms of domain geometry and imposition of waves at the seaward open boundary condition. This is mainly because DualSPHysics, with its closed domain boundaries, required the elaboration of a conduit for the

recirculation of overtopping water and also the derivation of the wavemaker motion from a wave signal. In terms of computational time, SWASH executed much faster (minutes) while DualSPHysics was computationally more expensive (hours), although the latter provided more details of the flow.

Lastly, the structure and foreshore considered in this paper were of relatively simple geometry and composition; more complex ones will be considered in future work in order to simulate more realistic scenarios. Particular focus will be given to the assessment of less conventional, more environmentally-friendly soft alternatives for the protection of shorelines against sea level rise-related effects.

## REFERENCES

- Battjes, J.A. 1974. Surf similarity, *Proceedings of 14<sup>th</sup> Int. Conf. on Coastal Engineering*, ASCE, 466-480.
- Casulli, V. and G.S. Stelling. 1998. Numerical simulation of 3D quasi-hydrostatic free-surface flows, *J. of Hydraulic Engineering*, 124, 678-686.
- Carvalho, M.M. 1989. Sea wave simulations, in Martins, R., *Recent advances in Hydraulic physical modeling*, Kluwer Academic Publishers, Dordrecht, The Netherlands, pp. 447-502.
- Crespo, A.J.C., J.M. Dominguez, M. Gómez-Gesteira, M. Barreiro, P., B.D. Rogers, S. Longshaw, R. Canelas and R. Vacondio. 2013. User guide for DualSPHysics Code v3.0.
- Dalrymple, R.A. and O. Knio. 2001. SPH modelling of water waves, *Proceedings of 4<sup>th</sup> Conference on Coastal Dynamics*, ASCE, 749-778.
- Dalrymple, R.A. and B.D. Rogers 2006. Numerical modeling of water waves with the SPH method, *Coastal Engineering*, 53, 141-147.
- Didier, E. and M.G. Neves. 2009. Coastal flow simulation using SPH: Wave overtopping on an impermeable coastal structure, *Proceedings of 4<sup>th</sup> International SPHERIC Workshop*.
- Didier, E. and M.G. Neves. 2010. A Lagrangian Smoothed Particles Hydrodynamics - SPH - method for modelling wave-coastal structure interaction, *Proceedings of 5<sup>th</sup> European Conference on Computational Fluid Dynamics*.
- Hibberd, S. and D.H. Peregrine. 1979. Surf and run-up on a beach: a uniform bore, *J. of Fluid Mechanics*, 95, 323-345.
- Lamont, G., J. Readshaw, C. Robinson, and P. St-Germain. 2014. Greening shorelines to enhance resilience – An evaluation of approaches for adaptation to sea level rise, guide prepared by SNC-Lavalin Inc. for the Stewardship Centre for British Columbia, Canada, and submitted to the Climate Change Impacts and Adaptation Division, Natural Resources Canada (AP040), 46p.
- Monaghan, J.J. 1994. Simulating free surface flows with SPH, *J. of Computational Physics*, 110, 399-406.
- Monaghan, J.J. and A. Kos. 1999. Solitary waves on a Cretan Beach, *J. of Waterway, Port, Coastal and Ocean Engineering*, 125, 145-154.
- Oliveira, T.C.A., A. Sánchez-Arcilla, and X. Gironella. 2012. Simulations of wave overtopping of maritime structures in a numerical wave flume, *Journal of Applied Mathematics*, Volume 2012, Article ID 246146, 19 pages.
- Stansby, P.K. and J.G. Zou. 1998. Shallow-water flow solver with non-hydrostatic pressure: 2D vertical plane problems, *Int. J. Numerical Methods in Fluids*, 28, 514-563.
- Stansby, P.K. 2003. Solitary wave runup and overtopping by a semi-implicit finite-volume shallow-water Boussinesq model, *J. Hydraulic Research*, 41, 639-648.
- Stansby, P.K. and T. Feng. 2004. Surf zone wave overtopping a trapezoidal structure: 1-D modeling and PIV comparison, *Coastal Engineering*, 51, 483-500.
- Stelling, G.S. and Zijlema, M. 2010. Numerical modeling of wave propagation, breaking and run-up on a beach, in Koren, B. and Vuik, C., *Advanced Computational Methods in Science and Engineering*, Springer-Verlag, Berlin, Germany, pp. 373-401.
- Verlet, L. 1967. Computer experiments on classical fluids. I. Thermodynamical properties of Lennard-Jones molecules, *Physical Review*, 159, 98-103.
- Wendland, H. 1995. Piecewise polynomial, positive definite and compactly supported radial functions of minimal degree, *Advances in Computational Mathematics*, 4, 389-396.
- Zijlema, M. and G.S. Stelling. 2008. Efficient computation of surf zone waves using the nonlinear shallow water equations with non-hydrostatic pressure, *Coastal Engineering*, 55, 780-790.
- Zijlema, M., G.S. Stelling and P. Smit 2011. SWASH: An operational public domain code for simulating wave fields and rapidly varied flows in coastal waters, *Coastal Engineering*, 58, 992-1012.